doi:10.1017/S1431927622005141
Microsc. Microanal. 28 (Suppl 1), 2022

Effects of Chameleon Dispense-to-Plunge Time on Grid Characteristics, Sample Distribution, and Complex Denaturation of the *Neisseria gonorrhoeae* Ribonucleotide Reductase Inactive Complex

Talya S. Levitz[1], Edward J. Brignole[1,2], Ivan Fong[3], Michele C. Darrow[3], and Catherine L. Drennan[1,4,5*]

[1.] Department of Biology, Massachusetts Institute of Technology, Cambridge, MA, USA.
[2.] MIT.nano, Massachusetts Institute of Technology, Cambridge, MA, USA.
[3.] SPT Labtech, Melbourn Science Park, Cambridge Rd, Melbourn, UK.
[4.] Department of Chemistry, Massachusetts Institute of Technology, Cambridge, MA, USA.
[5.] Howard Hughes Medical Institute, Cambridge, MA, USA.
* Corresponding author: cdrennan@mit.edu

Cryogenic electron microscopy (cryo-EM) is a leading technique for determination of the structure of proteins and protein complexes. However, preparation and freezing of cryo-EM grids is often an iterative process and generation of grids that produce high quality data sets is difficult if not impossible for some proteins, particularly those that display pathological preferred orientation or air/water interface denaturation [1–4]. Conventional plunging techniques, which involve contacting one or both sides of the grid with a blotting paper, generate thousands of air/water interface interactions per protein during the plunging process in addition to denaturation effects from the blotting paper itself [5–7]. In recent years, an explosion of next-generation cryo-EM sample preparation instruments have been generated or manufactured, ranging from in-house models such as the Back-it-up [8] to commercially available models such as the chameleon (developed by SPT Labtech and based on the Spotiton developed by Carragher et al.) [9–11]. The chameleon utilizes a piezoelectric dispenser and self-wicking nanowire grids with a tunable dispense-to-plunge time based on strength and duration of glow discharge; this allows for a blot-free device that can accommodate a range (2500 – 54 ms) of dispense-to-plunge times.

We recently published a paper detailing how we were able to obtain a cryo-EM structure of the *Neisseria gonorrhoeae* ribonucleotide reductase (RNR) in the inactive state with the use of the chameleon and a short (54 ms) dispense-to-plunge time [12]. RNR is the only known enzyme to convert ribonucleotide substrates into their deoxyribonucleotide products. This is a critical reaction for organismal DNA biosynthesis and repair; because of the essential nature of the enzyme, ribonucleotide reductase is a promising antibacterial drug target and is already the target of clinically used anti-cancer drugs. Recent research has indicated that the *N. gonorrhoeae* RNR (*Ng*RNR) is an especially promising bacterial drug target. *N. gonorrhoeae* contains a single RNR in its genome and impairment or inactivation of the enzyme leads to death for the organism [13]. Additionally, there have been recent discoveries of two small molecules that inhibit the gonorrheal RNR both in vitro and in vivo [14]. Importantly, these small molecules do not inhibit the human RNR, likely because of the human and gonorrheal RNRs having oligomerically distinct inactive states [14]. However, to further probe potential drug binding areas of ribonucleotide reductase, more structural data at a higher resolution were needed.

We were able to systematically analyze (1) particle distribution on grids, (2) the extent of *Ng*RNR inactive complex denaturation, and (3) the final resolution of *Ng*RNR inactive complex structures using different dispense-to-plunge times on the chameleon as compared to a Vitrobot-plunged control. We found that particle concentrations decreased with shorter dispense-to-plunge times, but that shorter dispense-to-plunge times actually had particle concentrations on the grid that more closely mirrored

those found in solution. Additionally, we were able to determine that, for the *Ng*RNR inactive complex, shorter dispense-to-plunge times led to fewer denatured particles and a greater percentage of particles that were able to be utilized in the final reconstruction (Figure 1). We were further able to process these data and determine that, after normalization to the same number of particles per data set, the sample plunged using the chameleon at the shortest dispense-to-plunge time processed to the highest resolution possible with the chosen imaging parameters; furthermore, a comparison of larger data sets taken on a grid plunged using the chameleon at the shortest (54 ms) dispense-to-plunge time versus a grid plunged using the Vitrobot found that a pixel-size-limited structure was attainable only by using a grid plunged on the chameleon at the shortest dispense-to-plunge time (Figure 2).

This study adds to the growing body of research around the forces and effects that occue on the nanoscale during the plunge freezing process. In addition, the findings here are relevant for any chameleon users and are applicable to many other next-generation cryo-EM sample preparation instruments. Through this detailed case study of the *Ng*RNR inactive complex, we provide a roadmap for how other proteins could be analysed in order to find optimal plunging conditions based on challenges seen early on in screening or processing. Additionally, *Ng*RNR is a biochemically complex protein and potential drug target from a pathogenic organism, opening up new biochemical and drug development options from the presented structure and a demonstration of the benefits of chameleon use with a “real world” sample.

https://doi.org/10.1017/S1431927622005141 Published online by Cambridge University Press

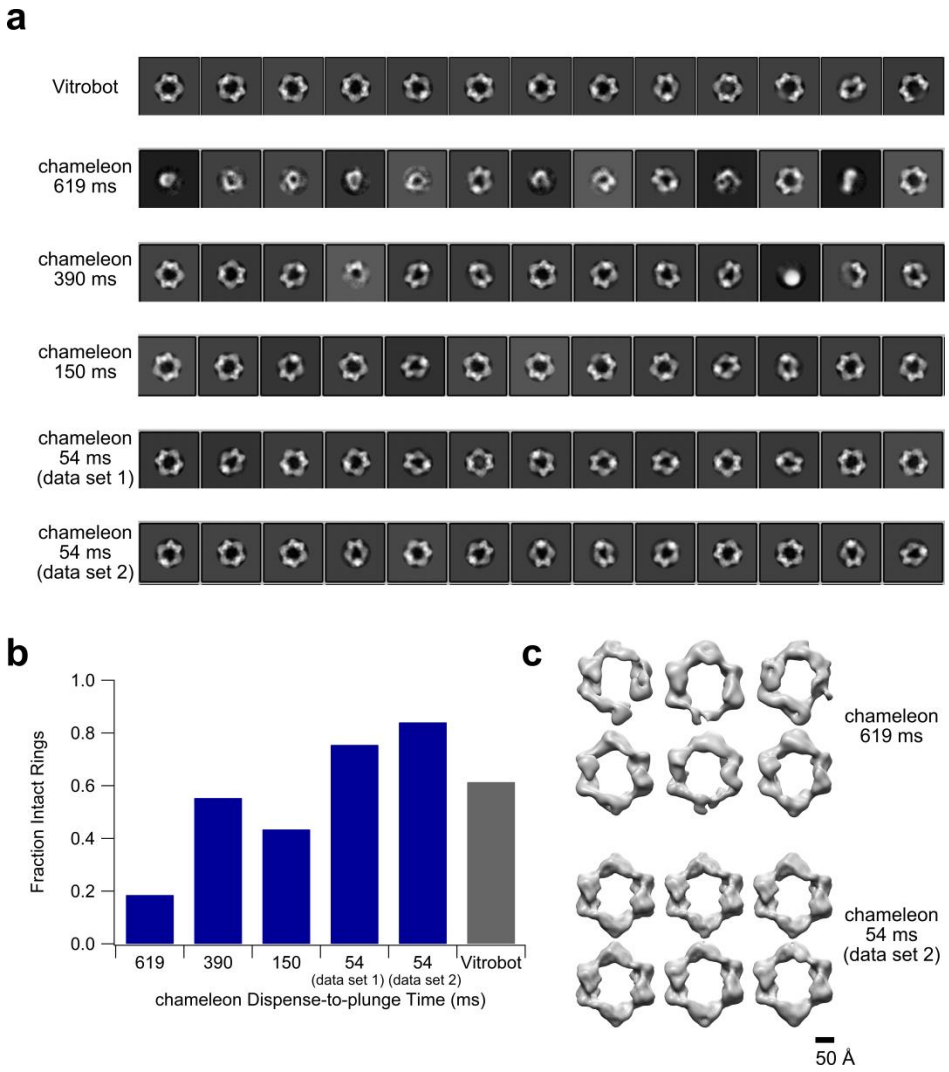

Figure 1. Shorter chameleon dispense-to-plunge times result in less particle denaturation. (a) The top thirteen 2D classes for each data set taken. The total number of 2D classes calculated for each sample was 200. (b) The fraction of particles contributing to 2D classes that contained intact rings versus the total number of particles in classes containing intact or broken rings for each data set. Ambiguous classes (i.e. side views where the intact state of the particles could not be determined) and non-ring-shaped classes were excluded from the analysis. (c) 3D classes for the chameleon 619 ms and 54 ms (data set 2) dispense-to-plunge time data sets. Six classes and 100 rounds of classification were specified for each data set. Particle inputs to the 3D classification were those that contributed to 2D classes consisting of intact rings or ambiguous side views in each of two rounds of 2D classification. Figure and caption from [12].

https://doi.org/10.1017/S1431927622005141 Published online by Cambridge University Press

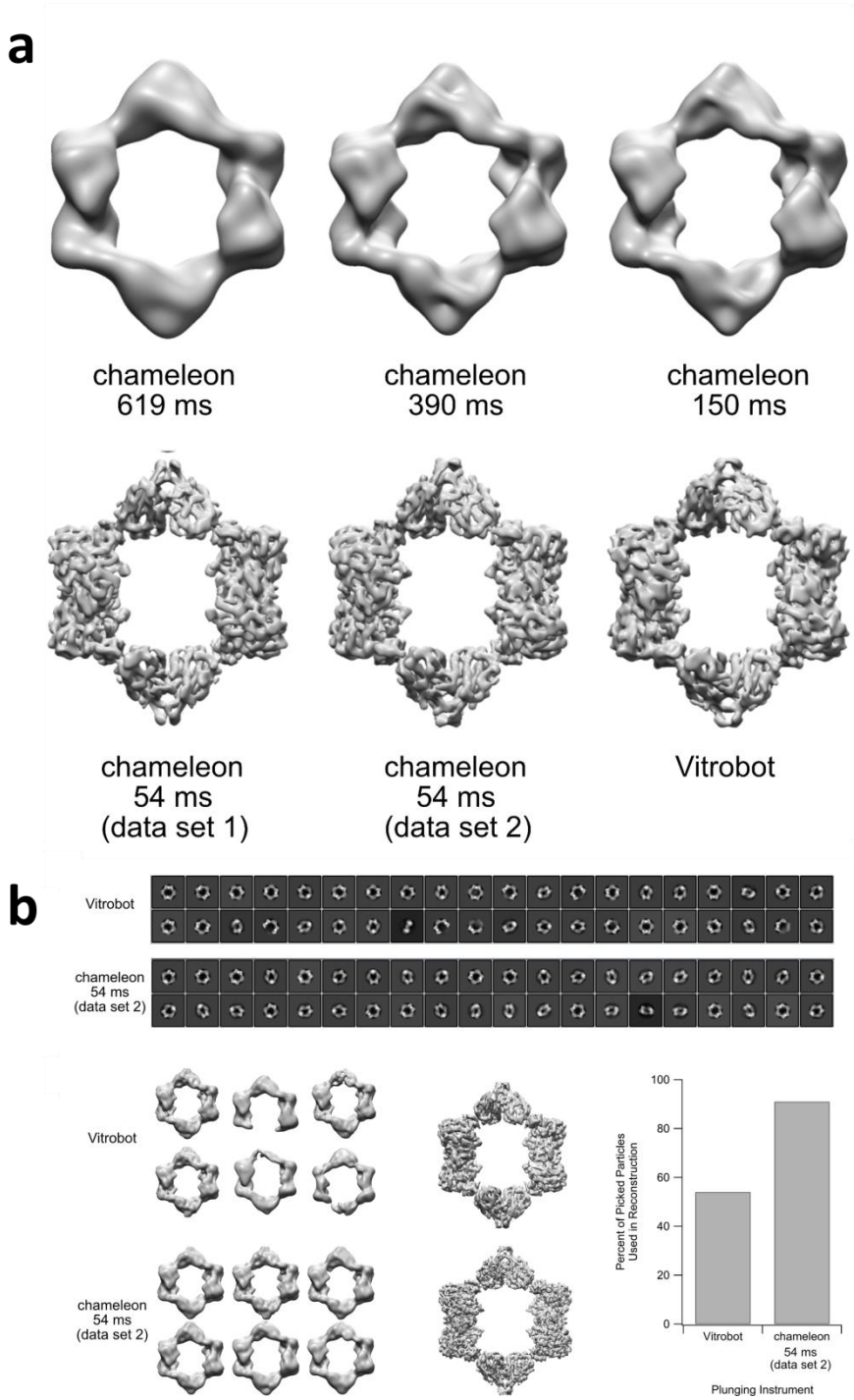

Figure 2. The chameleon at a short dispense-to-plunge time is necessary for a high resolution structure of the *Ng*RNR inactive state. (a) Decreasing chameleon dispense-to-plunge time increases resolution of the final reconstruction. The plunging instrument and dispense-to-plunge time (where applicable) are indicated below each structure. Each structure was generated using 7942 particles randomly selected from all particles remaining after the 3D classification step. All structures are shown after postprocessing in Relion 3.1 at an RMSD value of 6. The final resolutions of each data set are 23 Å, 21 Å, 18 Å, 10 Å, 7.3 Å, and 8.7 Å resolution, reading left to right, top to bottom across the figure. (b) A

https://doi.org/10.1017/S1431927622005141 Published online by Cambridge University Press

chameleon grid plunged using a 54 ms dispense-to-plunge time produced a data set that processes better and more efficiently than a data set produced from a Vitrobot-plunged grid. (top) Top 40 2D classes (of 200 total classes) of data sets from a Vitrobot-plunged grid and a chameleon-plunged grid. 2D classes were generated using 25 iterations in Relion. (bottom left) 3D classes generated from the Vitrobot-plunged grid and the chameleon-plunged grid. Six classes and 100 rounds of classification were specified in Relion for each data set. Particle inputs to the 3D classification were those that contributed to 2D classes consisting of intact rings or ambiguous side views in each of two rounds of 2D classification. All classes are visualized at an RMSD value of 6. (bottom middle) Postprocessed reconstructions of the data from the Vitrobot-plunged grid (top) and a chameleon-plunged grid (bottom). Reconstructions are at 5.6 Å and 4.3 Å resolution, respectively. Both reconstructions are visualized at an RMSD value of 6. (bottom right) Comparison of the percentage of initially-picked particles (at 95% recall in Topaz) that were used to generate the final reconstruction for the data sets generated from the Vitrobot-plunged grid and the chameleon-plunged grid. Figures and caption from [12].

References:

[1] D. Lyumkis, J Biol Chem **294** (2019) p. 5181–5197.
[2] R.M. Glaeser, Curr Opin Colloid Interface Sci **34** (2018) p. 1–8.
[3] A.J. Noble et al., eLife **7** (2018) e34257.
[4] A.J. Noble et al., Nat Methods **15** (2018) p. 793–795.
[5] M. Armstrong et al., Biophysical Journal **118** (2020) p. 708–719.
[6] E. D'Imprima et al., eLife **8** (2019) e42747.
[7] K.A. Taylor, R.M. Glaeser, J Struct Biol **163** (2008) p. 214–223.
[8] Y.Z. Tan, J.L. Rubinstein, Acta Cryst D **76** (2020) p. 1092–1103.
[9] T. Jain et al., J Struct Biol **179** (2012) p. 68–75.
[10] M.C. Darrow et al., Microscopy and Microanalysis **25** (2019) p. 994–995.
[11] H. Wei et al., Microscopy and Microanalysis **25** (2019) p. 1010–1011.
[12] T.S. Levitz et al., Journal of Structural Biology **214** (2022) p. 107825.
[13] C.W. Remmele et al., Nucleic Acids Res **42** (2014) p. 10579–10595.
[14] J. Narasimhan et al., eLife **11** (2022) e67447.

https://doi.org/10.1017/S1431927622005141 Published online by Cambridge University Press